Journal of Power Sources 309 (2016) 169–177

Contents lists available at ScienceDirect

Journal of Power Sources

journal homepage: www.elsevier.com/locate/jpowsour

Synergetic effects of $LiFe_{0.3}Mn_{0.7}PO_4$–$LiMn_{1.9}Al_{0.1}O_4$ blend electrodes

Andreas Klein*, Peter Axmann, Margret Wohlfahrt-Mehrens

ZSW – Zentrum für Sonnenenergie- und Wasserstoff-Forschung, Baden-Württemberg, Helmholtzstrasse 8, D-89081 Ulm, Germany

HIGHLIGHTS

- Positive synergetic effects are observed for LFMP-spinel blends.
- Potential stability is improved during high current loads compared to pure LFMP.
- Electrode polarization is strongly reduced in LFMP-spinel blends.
- Power density of blends exceeds that of single components at high rates and SoC.
- Spinel-related manganese dissolution can be drastically reduced.

GRAPHICAL ABSTRACT

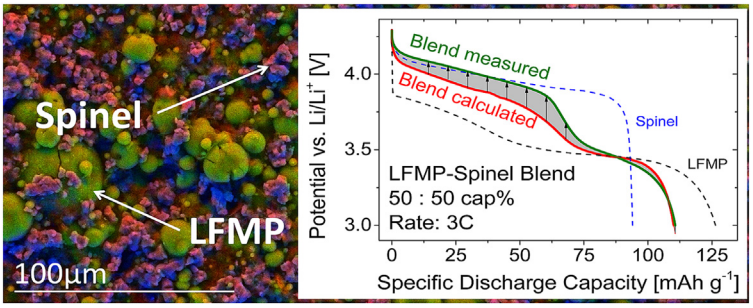

ARTICLE INFO

Article history:
Received 20 November 2015
Received in revised form
14 January 2016
Accepted 25 January 2016
Available online 5 February 2016

Keywords:
Lithium-ion batteries
Cathode
$LiFe_{0.3}Mn_{0.7}PO_4$
Spinel
Blend
Synergetic effects

ABSTRACT

Composite cathodes are prepared by blending the olivine $LiFe_{0.3}Mn_{0.7}PO_4$ (LFMP) and spinel $LiMn_{1.9}Al_{0.1}O_4$ (LMO) in order to combine the high capacity of LFMP with the rate capability of the spinel. While tap density, capacity and energy density show a linear dependency on the blend ratio, a remarkable synergetic effect between LFMP and LMO improving the electrochemical performance at higher C-rates is demonstrated. Potential curves of blend electrodes at rates of 3C reveal a less pronounced polarization for the $Mn^{2+/3+}$ plateau than expected from theoretical calculations. This buffer effect is also observed for high current pulses (5C) where blend electrodes resemble the behavior of pure spinel electrodes. In terms of power density at high states of charge (SoC), the performance of the Blend($50_{LFMP}/50_{LMO}$ cap%) exceeds even that of pure spinel. In addition, the spinel-related manganese dissolution can be drastically reduced by blending spinel with LFMP. This study shows the expected and synergetic effects of LFMP/spinel blends and compares the results with theoretical calculations.

1. Introduction

Lithium-ion battery (LIB) technology is the key enabler of energy storage and electric propulsion. Today's LIB technology was primarily developed for applications in consumer electronics and is now transferred into automotive applications. These applications demand high specific capacity in order to provide a long driving range as well as high power densities for acceleration, recharging and regeneration.

So far, state-of-the-art Lithium-ion batteries do not fully meet the requirements of automotive applications with respect to energy density, power density, extended lifetime, cost and safety. Among the commercially used active cathode materials, the lithium metal phosphates are promising compounds with respect to power, lifetime and safety. The commercialized $LiFePO_4$ exhibits good rate capability. Energy density is below that of commercially used layered oxides due to its redox plateau at 3.5 V. A lot of interest is

* Corresponding author.
E-mail addresses: andreas.klein@zsw-bw.de (A. Klein), peter.axmann@zsw-bw.de (P. Axmann), margret.wohlfahrt-mehrens@zsw-bw.de (M. Wohlfahrt-Mehrens).

http://dx.doi.org/10.1016/j.jpowsour.2016.01.093

therefore drawn to the isostructural $LiMnPO_4$ due to its higher redox plateau of 4.1 V vs. Li/Li^+, which is able to provide higher energy densities [1,2]. Unfortunately, pure $LiMnPO_4$ suffers from low rate capability.

On material level, Yamada et al. demonstrated that the partial substitution of manganese in $LiMnPO_4$ with iron, $Li(Mn_xFe_{1-x})PO_4$ (LFMP) leads to improved electrochemical performance and increased energy density [3,4]. On electrode level, a promising strategy to further adjust the electrochemical behavior is to custom-tailor properties by blending complementary types of cathode materials [5–7]. In order to enhance the limited kinetics of manganese based olivine, blending with $LiMn_2O_4$-spinel is expected to result in a promising cathode material for two reasons: a) spinels show fast kinetics, as can be observed from a less pronounced electrode polarization at higher C-rates and b) provide a redox plateau in a range comparable to LFMP. On this basis, our approach was to use spinel as component with fast kinetics to buffer the voltage drop of LFMP for current pulses or higher C-rates. From a technical point of view, further advantages provided by the spinel are inexpensive raw material cost and high thermal stability in the charged state [8–10]. The spinel is reported however to show lower cycle life due to manganese dissolution [11–14]. This can be improved by doping with aluminum [15,16].

In this work, we investigate the influence of blending $LiFe_{0.3}Mn_{0.7}PO_4$ (LFMP) with $LiMn_{1.9}Al_{0.1}O_4$ (spinel) on the electrochemical behavior and compare the results with theoretical calculations. Electrode kinetics are investigated via pulse power tests at different base current rates and different depths of discharge (DoD).

2. Experimental

2.1. Material characterization

Structural characterization (X-ray Diffraction) was performed on a Siemens D5000 X-ray powder diffractometer using Cu-Kα radiation ($\lambda = 0.154$ nm). The diffraction data were obtained in a range of $10° \leq 2\Theta \leq 120°$, with a step size of 0.03° per step. Phase analysis was carried out with the evaluation software EVA. Scanning Electron Microscopy (SEM) images and Energy Dispersive X-ray Spectrometer mappings (EDX) were obtained on a LEO 1530VP.

2.2. Preparation

$LiFe_{0.3}Mn_{0.7}PO_4$ with 2.9 wt% of carbon content (Johnson Matthey Battery Materials GmbH) and 10 wt% Al-doped spinel $LiMn_{1.9}Al_{0.1}O_4$ (pre-commercial material) were mechanically mixed in different ratios and grounded in a mortar. The mass ratios were set to result in blend materials which provide a capacity ratio in percent (cap%) of 50_{LFMP}:50_{LMO} and 67_{LFMP}:33_{LMO} based on experimentally obtained data of pure LFMP and spinel at 0.1C. All electrodes were prepared from a slurry containing active material, carbon additive (Super-P, Timcal), graphite (SFG6L, Timcal), polyvinylidene fluoride binder (P5130, Solvay Solexis) in the ratio 86:4:4:6 wt%. The slurry was coated on an aluminum foil current collector using a doctor blade technique. The wet film thickness was adjusted to result in a comparable electrode loading of 1.50 ± 0.05 mAh cm^{-2}. After drying at 60 °C for 2 h, the coated current collector was stored under vacuum overnight. Circular electrodes were punched from the foil, pressed (8 t, 1 min, 25 °C) and dried at 130 °C overnight. The electrochemical measurements were performed using Swagelok-type cells in a three electrode arrangement. Cells were assembled in an argon-filled glove box. Metallic lithium was used as anode and as reference electrode (Sigma Aldrich), glass microfiber (Whatman, GF/A) with a pore size of 1.6 μm and a thickness of 0.26 mm as separator and 1 M $LiPF_6$ in EC:DMC 1:1 by weight from Ube Industries, Japan as electrolyte.

2.3. Electrochemistry

The electrochemical characterization was divided into two parts: rate capability tests and pulse power tests. Experimental results have been compared with calculations assuming pure physical mixtures of LFMP and spinel without any particle-to-particle interaction. For the rate capability test, a defined C-rate profile was applied: 0.1C, 0.2C, 1C, 2C, 3C and again 0.1C. At each C-rate, three galvanostatic cycles have been collected. C-Rates were calculated based on the experimental capacity at rates of 0.1C for each material, respectively. All electrochemical measurements were performed at 25 °C using a BaSyTec electrochemical workstation. All potentials are given in V vs. Li/Li^+.

A detailed description of the method used to calculate the galvanostatic curves of hypothetical blend electrodes can be found in the supplementary information. Calculations of expected values, both for gravimetric energy and power density, were based on the galvanostatic curves obtained from rate capability measurements. In order to investigate the electrode polarization, pulse power tests were performed. In accordance with the rate capability tests, a cycle at 0.1C served as reference. Three different C-rates 0.1C, 1C and 3C have been applied as base currents for discharging in order to investigate the influence of high current pulses at different base electrode polarizations. The cells were discharged in steps of 10% DoD. After each step, a 5C pulse was applied with subsequent relaxation period of 90 min.

3. Results and discussion

3.1. General characterization

For a given active material, the electrode performance is strongly dependent on factors such as composition and porosity of the electrode composite, and the active mass loading. Morphological features of the active material play an additional role as they can influence the grain packing and thereby the density of the electrode composite. In order to obtain a first hint on processing behavior, tap densities of the pure and mixed powders are investigated. Table 1 lists the tap densities of all used materials and the expected theoretical values for the blend materials. Relating to LFMP and spinel (LMO), a linear dependency of the tap density on the composition is observed. This means electrode density can be predicted according to the spinel content in the blend which allows an easier adjustment of electrode parameters. Further characterizations of the cathode materials and electrodes can be found in the supplementary information.

Both specific capacity as well as electrode potential contribute to the energy density via the relation $E = Q \cdot U$ (E = Energy, Q = Capacity, U = Potential). Additionally to the capacity, the working potential is a characteristic parameter which needs to be taken into account. Fig. 1a shows the influence of C-rate on the capacity of LFMP. The coulombic efficiency is about 99.8%. Significant deviations in efficiency when changing the C-rates can be observed. These deviations are due to changes in material utilization related to the change in electrode polarization.

Pure LFMP shows an initial capacity at 0.1C of 143 mAh g^{-1}, which is reduced slightly with increasing C-rate. At 3C, 88% of the initial capacity can still be obtained, demonstrating high rate capability with respect to the coulombic utilization. After the rate capability test ending at 3C, the initial capacity of 143 mAh g^{-1} at 0.1C can be fully retained, indicating no material degradation even at higher rates. However, significant changes in the voltage

Table 1
Tap density of LFMP, spinel and both blends compared with calculated values assuming no synergetic effects.

Material	LMO content wt%	LMO content capacity %	Tap density g mL^{-1}
$LiMn_{1.9}Al_{0.1}O_4$	100	100	1.90
$LiFe_{0.3}Mn_{0.7}PO_4$	0	0	1.41
Blend($50_{LFMP}/50_{LMO}$ cap%)	57.9	50	1.67
Blend($50_{LFMP}/50_{LMO}$ cap%)calc.	57.9	50	1.69
Blend($67_{LFMP}/33_{LMO}$ cap%)	40.5	33	1.58
Blend($67_{LFMP}/33_{LMO}$ cap%) calc.	40.5	33	1.60

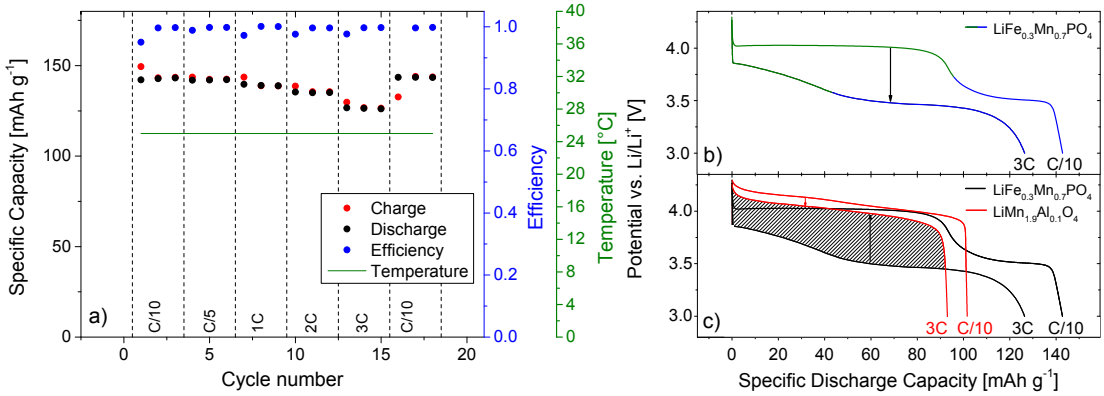

Fig. 1. a) Rate capability measurement of LFMP and b) galvanostatic curves of LFMP at 0.1C and 3C. c) Galvanostatic curves of LFMP and spinel at 0.1C and 3C depicting where a buffer effect can be expected (shaded area).

characteristics can be observed at high C-rates (Fig. 1b). A pronounced voltage drop of about 600 mV for the $Mn^{2+/3+}$ redox plateau (green) can be detected which significantly lowers energy density at elevated C-rates. This strong polarization suggests slow kinetics for the $Mn^{2+/3+}$ redox step. Furthermore, the initial two-step behavior related to the $Mn^{2+/3+}$ (higher plateau) and $Fe^{2+/3+}$ (lower plateau) steps changes significantly with respect to the plateau lengths for higher C-rates. At 3C, the lower plateau shows an extended length while the higher plateau is shortened. The ratio of the individual lengths shifts and does not further correspond to the theoretical expectation of the Mn^{2+}:Fe^{2+} ratio. This indicates that part of the manganese ions are discharged on the lower plateau and both redox pairs overlap to a certain extent.

3.2. Concept

There are several options to influence the kinetics of an electrode. For LFMP our approach is to investigate whether the potential drop depicted in Fig. 1b can be buffered by adding spinel (LMO). The approach is based on the following: the $Mn^{2+/3+}$ redox plateau of the investigated $LiFe_{0.3}Mn_{0.7}PO_4$ and the $Mn^{3+/4+}$ plateau of spinel overlap in terms of their potential range at around 4 V, but much faster kinetics are observed for the spinel. The expected improvement is to be associated with the distribution of the effective C-rate onto the two materials assessed according to their kinetics and ratio in the electrode. This would mean a higher proportion of the current will be utilized for the material with fast kinetics and a lower proportion for the one with slower kinetics. This may result in a less polarized electrode.

Fig. 1c shows the galvanostatic curves of LFMP and spinel at 0.1C and 3C. With increasing C-rate, the potential drop of a pure spinel electrode between 0.1C and 3C is only 100 mV whereas for LFMP a well pronounced electrode polarization results in a voltage drop of 600 mV on the manganese plateau. The grey shaded area between the curves of LFMP and spinel at 3C illustrates the range where a buffer effect could be expected. At low C-rates, both materials are expected to be discharged according to their individual redox potentials. The behavior of the blend electrode consisting of LFMP and LMO can be calculated by assessed summation of capacities in equally spaced potential steps. We assume that any deviation between experimental galvanostatic curves and calculated ones are assigned to a reduction of electrode polarization or a possible particle-to-particle interaction.

3.3. Rate capability

The galvanostatic curves of pure LFMP, Blend($67_{LFMP}/33_{LMO}$ cap %), Blend($50_{LFMP}/50_{LMO}$ cap%) and pure spinel at different C-rates are arranged in Fig. 2. As previously mentioned, for electrodes of pure LFMP (Fig. 2a), the dependency of electrode potential from C-rate is well pronounced both for charging and discharging. For charging, the polarization of the LFMP electrode reaches the cut-off criterion (4.3 V) at an early state of charge (SoC). This requires a constant voltage (CV) step in order to complete the charge uptake. The galvanostatic curves of Blend($67_{LFMP}/33_{LMO}$ cap%) and Blend($50_{LFMP}/50_{LMO}$ cap%) (Fig. 2c and d) show a less pronounced polarization on the manganese plateau compared with LFMP. Blend($50_{LFMP}/50_{LMO}$ cap%) exhibits an even less pronounced voltage drop compared with pure spinel (Fig. 2b). The reduced voltage drop at high rates in combination with observed shorter CV-steps during charging gives an indication of a reduced electrode polarization at elevated C-rates and improved kinetics between 4.3 and 3.8 V.

Potential curves of blend electrodes are calculated based on individually measured galvanostatic curves of LFMP and spinel, comparable to calculations described by Schmidt et al. [17]. The calculations represent galvanostatic curve characteristics of a hypothetical blend assuming pure physical mixtures without any interactions between both active materials. For the comparison of experimental and theoretical data, blend electrodes with

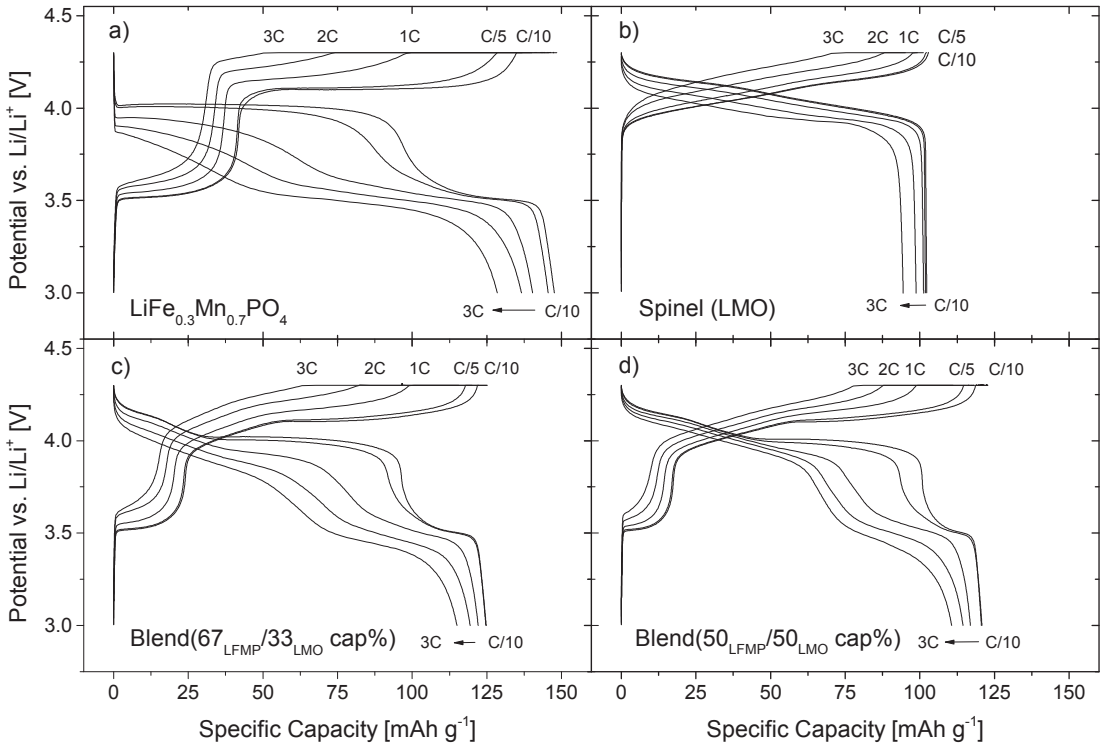

Fig. 2. Galvanostatic Curves of a) LFMP, b) spinel, c) Blend($67_{LFMP}/33_{LMO}$ cap%) and d) Blend($50_{LFMP}/50_{LMO}$ cap%) obtained from rate capability measurement.

comparable loading in terms of capacity are necessary. During charge and discharge of a blend electrode, capacity ranges alternate, in which either both or the single components are electrochemically active. The degree to which each component electrochemically contributes at a certain state of charge of the overall blend depends on its individual potential curve, which again is dependent on the C-rate. Therefore, the C-rate applied to a blend electrode does not directly correlate with the effective C-rate on the individual components. The effective C-rate on one single component in a blend electrode can be defined as the C-rate times the ratio of the component.

This applies, however, only to low rates and overlapping operating windows of both components in terms of capacity. At higher rates, synergetic effects can be assumed for components with different kinetics. This can be seen if current distribution on the materials differs from their expected distribution, according to the ratio in the blend. If there is only one active component, the effective C-rate results from the quotient of the applied C-rate and component ratio.

The calculated and measured galvanostatic curves from blend electrodes, as well as from LFMP and spinel are depicted in Fig. 3a–b. Differences in kinetics of calculated and measured blend electrodes are expected to be more pronounced at elevated C-rates. In order to illustrate these effects and to provide clarity, the galvanostatic curves in Fig. 3a–b are shown for one rate of 3C. For galvanostatic curves at low C-rates see Fig. S4 in the supplementary information. Solely regarding the specific discharge capacities, both blends are performing, as expected, like physical mixtures of LFMP and spinel according to their ratios. In regards to the potential profile, an increased working potential can be observed for the experimental curve in the range between 4.3 and 3.6 V, as compared to the theoretical values. With increasing spinel content this effect is more pronounced. An explanation for this is on the one hand a reduced polarization due to a higher current distribution on the spinel than expected from the product of applied C-rate and the ratio of spinel, and on the other hand a possible charge exchange between spinel and LFMP particles. These effects may interfere with each other and cannot be separated. The potential of the iron plateau (~3.5 V) of both blends as depicted in Fig. 3a–b shows a slight potential drop, as compared to the calculated values and can be related to the change in effective C-rate. The reason for this behavior is that the $Fe^{2+/3+}$ redox pair of LFMP in the blend is working outside the operating window of the spinel, which results in an increased current rate on LFMP according to the quotient of applied C-rate and ratio of LFMP. The effective C-rate on LFMP during discharging the iron plateau (3.5 V) can be calculated to 6C for the Blend($50_{LFMP}/50_{LMO}$ cap%) and 4.5C for Blend($67_{LFMP}/33_{LMO}$ cap%). A higher potential in the 4 V region and a less pronounced potential drop in the 3.5 V region than expected indicates faster kinetics and suggests lower electrode polarization, which may also be attributed to possible particle-to-particle interaction.

A more detailed view on the calculated capacity contributions of the individual active materials to the blend capacities is demonstrated in Fig. 3c–d, showing derivative plots of an LFMP, a spinel and the corresponding blend electrodes. For this plot the derivatives $dQ\,dE^{-1}$ vs. E have been transferred to a $dQ\,dE^{-1}$ vs. Q. The capacity Q has been calculated for equally spaced potential steps of $\Delta E = 10$ mV. The area below the orange, green and blue curves corresponds to the obtained capacities of the materials. The expected working range of LFMP and spinel according to the amount used in Blend($50_{LFMP}/50_{LMO}$ cap%) and Blend($67_{LFMP}/33_{LMO}$ cap%) are calculated based on measurements of electrodes from pure LFMP and pure spinel, respectively. In Blend($50_{LFMP}/50_{LMO}$ cap%), the operating window of LFMP and spinel can be expected to overlap in the DoD range between 40 and 66% as depicted in Fig. 3c. Comparing the shown derivatives of the blends with the derivatives of their pure components, we observe an increasing capacity contribution on the manganese plateau and a slightly decreasing

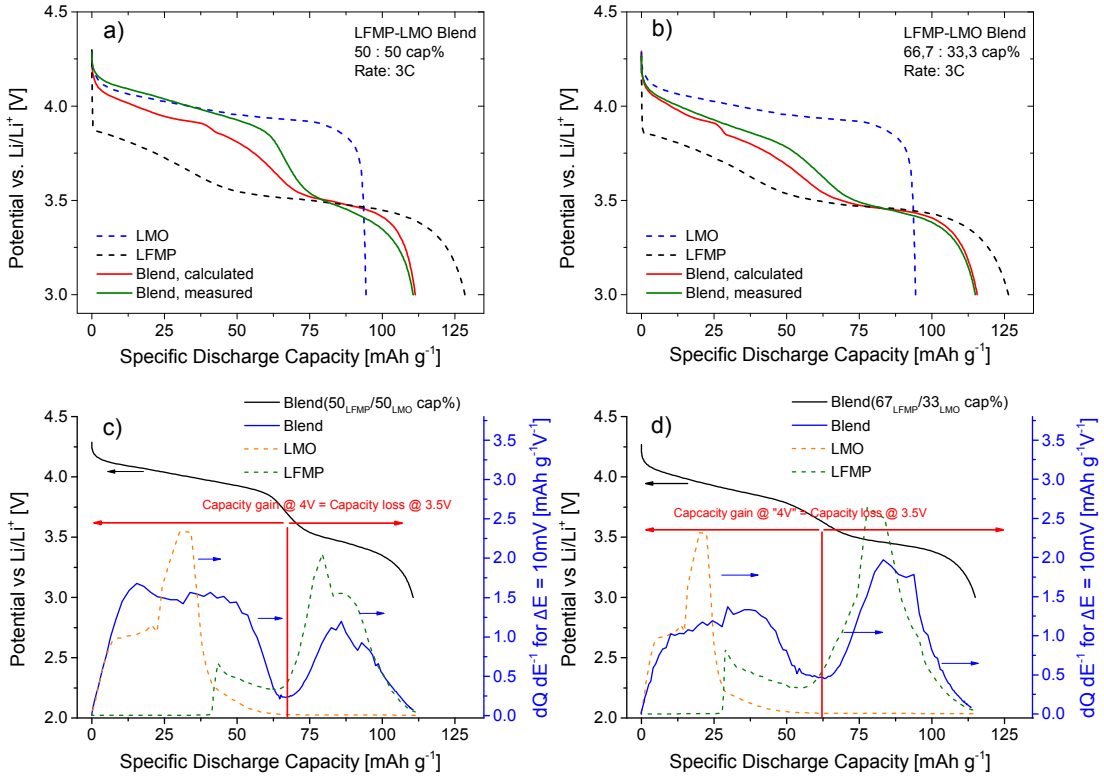

Fig. 3. Comparison of calculated and measured galvanostatic curves of a) Blend($50_{LFMP}/50_{LMO}$ cap%) and b) Blend($67_{LFMP}/33_{LMO}$ cap%) at 3C, respectively and the capacity contribution from LFMP and spinel to the blend capacity for c) Blend($50_{LFMP}/50_{LMO}$ cap%) and d) Blend($67_{LFMP}/33_{LMO}$ cap%) at rates of 3C, respectively.

contribution on the iron plateau. During discharge the capacity gain at the manganese redox step equals the capacity loss at the iron redox step at the change over from one to the other. The shifted capacity amounts to 16 mAh g^{-1}, which equates to 29% capacity as related to a pure LFMP electrode. This 29% of capacity is discharged at a higher potential (4 V instead of 3.5 V) than expected, which results in an increased energy density and power density as compared with a physical mixture of active materials, without any interaction between the materials. Comparable trends can be observed for Blend($67_{LFMP}/33_{LMO}$ cap%) with a lower spinel content. Interaction between LFMP and spinel can be expected in the range between 27 and 60% DoD as shown in Fig. 3d. An increased capacity contribution of 5.5 mAh g^{-1} can be detected on the manganese plateau. This equates to 7% capacity as related to LFMP which is discharged at higher potentials than expected from pure LFMP electrodes and cannot be only explained by pure physical mixtures.

The results show that tap density, electrode thickness, porosity and the total discharge capacity are well predictable according to the blend ratio. Synergetic effects can be observed in cases of electrode polarization and redox potential of the LFMP related manganese plateau at elevated C-rates. In addition, capacity contributions of manganese discharged at a lower redox plateau than expected can be partially regained at higher C-rates.

3.4. Energy density

According to the polarization of pure LFMP electrodes at elevated C-rates, the energy densities at these rates are comparably low. In order to visualize the influence of the blend ratio on the energy density at different C-rates, the difference in energy density between the blends and the pure spinel, as well as the pure LFMP is calculated. The energy densities of all materials are obtained via

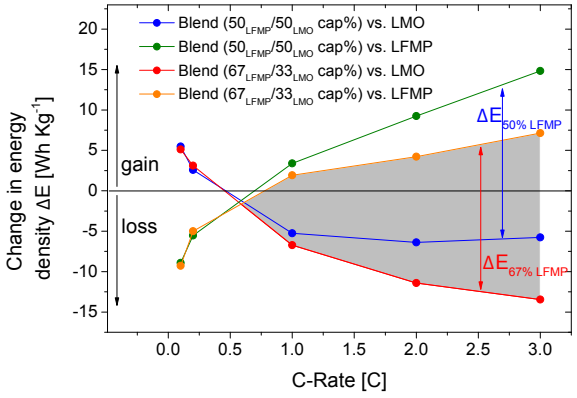

Fig. 4. Energy density of both blend electrodes at different C-rates related to 100% LFMP- and 100% spinel electrode.

integration of galvanostatic curves (in mAh g^{-1}) in a potential range between 4.3 and 3.0 V. Fig. 4 compares two different blend ratios with respect to their pure components. The orange and the red curve enclose a grey marked area and describe the behavior of Blend($67_{LFMP}/33_{LMO}$ cap%) while the green and the blue ones correspond to Blend($50_{LFMP}/50_{LMO}$ cap%). The curves with a positive slope represent a gain in energy density relating to pure LFMP while at the same time a mean negative slope stands for a loss of energy density referred to pure spinel. The curves can be divided into two sections. At low C-rates (<0.6C) the change in energy densities remains almost unaffected by the blend ratio. At higher C-rates (>0.6C) the curves diverge dependent on the blend composition. The slope of all curves increases with spinel content. It may be inferred that a rising spinel content can increase the gain in

energy density compared to pure LFMP and simultaneously minimize the loss versus pure spinel for C-rates > 0.6C. For a given composition, the difference between loss and gain of energy density $\Delta E_{LFMP\%}$ relating to spinel and LFMP shows a linear behavior according to the applied C-rate and can be described for both blends and rates >0.6C by a linear equation: $\Delta E_{LFMP\%} = 5.9$ C-rate + 3. In principle, it can be said, that the gap between of loss and gain in energy density related to the raw materials of this blend can be predicted according to the blend ratio and the applied C-rate.

3.5. Power density

While energy densities are calculated from the product of potential and capacity, the power densities are calculated from the quotient of energy densities and time. Values have been obtained at each state of discharge. The observed power densities are obtained from constant current measurements. Electrode characteristics at constant current differ from pulse power behavior which will be discussed later. Fig. 5 shows a general view of specific gravimetric power densities along the degree of discharge depending on the C-rate and blend composition. As reference, the pure materials are included for comparison. For the evaluation, two characteristic points are defined. Fig. 5a shows exemplarily how the data are collected. Point (A) describes the power density level which corresponds to 40% DoD of the blend electrode. At this point the manganese plateau of LFMP in the blend is discharged at both low and high rates (30–43% DoD). Point (B) marks the depth of discharge where the power density of the measured blend drops below that of the spinel. The theoretical power density curves are calculated based on the assumption that blends can be described as physical mixtures without any particle-to-particle interaction between the two active materials.

At rates of 0.1C, the measured power densities are in agreement with the theoretical calculations. Both active materials in the blend electrodes are discharged sequentially according to their redox plateaus. At low rates, the power densities for different blend ratios can be predicted according to the amount of added spinel. With increasing C-rate, the deviation between experimentally and

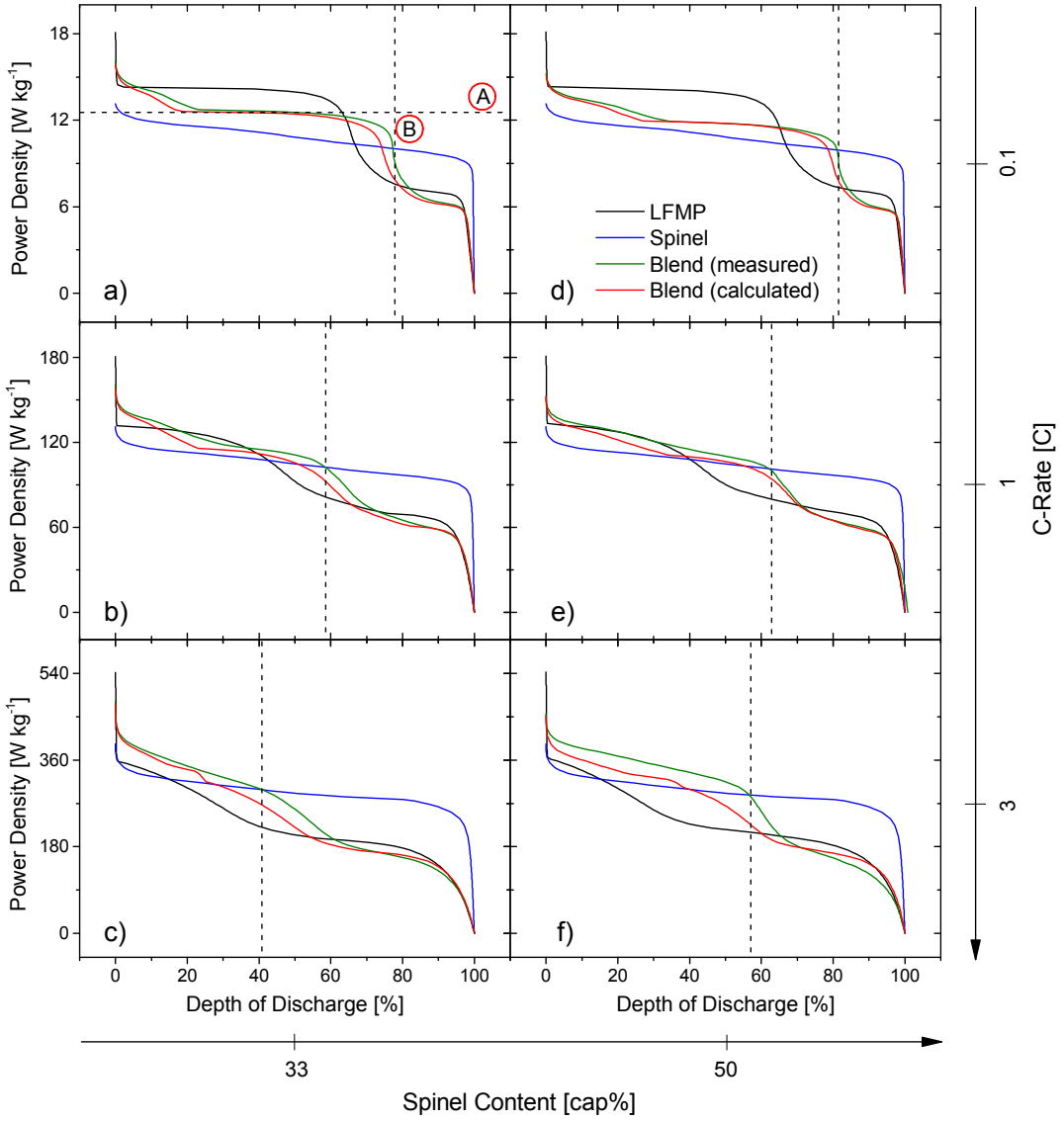

Fig. 5. Power density of LFMP, spinel, both blends and theoretical calculations at different C-rates. a–c) Blend($50_{LFMP}/50_{LMO}$ cap%) 0.1 C–3C and d) – f) Blend($67_{LFMP}/33_{LMO}$ cap%) 0.1 C–3C. Point (A) describes the power density level which corresponds to 40% DoD of the blend electrode and point (B) marks the depth of discharge where the power density of the measured blend drops below that of the spinel.

theoretically obtained power densities is more pronounced. The experimental blend curves indicate an increased power density during discharge of the manganese plateau (A) at elevated C-rates in comparison to the calculated ones. With increasing C-rate, point (B) shifts to lower depths of discharge while for a higher spinel/LFMP ratio, this behavior is less pronounced. The obtained power densities exceed the calculated values for pure physical mixtures, indicating less polarized electrodes. Such blend electrodes with high rate ability at high states of charge are interesting, for example, in the use of starter-batteries where the battery is at most times fully charged and high currents are required to start the internal combustion engine.

In summary, the energy density of blended LFMP and LMO can be tuned and accurately predicted for a given blend ratio. This allows designing cathode materials according to specific energy density requirements. Regarding the power densities at higher C-rates, experimental values exceed calculated ones at low DoD. With increasing spinel-content and C-rates, the observed positive synergetic effects are more pronounced leading to even higher electrode performance.

3.6. Pulse power tests

Pulse power tests are applied in order to analyze the influence of current pulses on the electrode potential according to their depth of discharge (DoD) during constant current discharge at different C-rates. This can give us indication about the prospective behavior in electric vehicles during fast acceleration or regeneration. In principle, Fig. 6 depicts the pulse power capability of both blends and single component materials depending on depth of discharge. Based on constant base current rates, pulses of 5C have been applied for 10 s respectively. The pulse power capability has been compared in intervals of 10% DoD. Fig. 6a depicts a schematic of the applied methodology and data collection. The values of the potential drop for LFMP at different DoD and at different base current rates are shown in Fig. 6b. Pulse power behavior can be inferred by evaluation of these curves. A maximum of the values can be observed between 30 and 60% DoD which is in the same range where the transition from the manganese to the iron plateau in potential curves is observed. The maximum shifts to lower DoD with increasing C-rate. The base discharge rate has a well pronounced impact on the magnitude of the potential drop of LFMP during the applied pulses. With increasing base C-rate, a decline in potential drop from the pulse can be observed. Fig. 6c–d compare Blend($50_{LFMP}/50_{LMO}$ cap%) and Blend($67_{LFMP}/33_{LMO}$ cap%) with the single component materials. The data are compared at base current rates of 0.1 and 3C in order to visualize the change in potential drop and DoD at low and high rates. In contrast to LFMP, a different behavior can be observed for the spinel electrodes. A maximum potential drop as found for the pure LFMP electrodes cannot be observed. Both blend electrodes resemble the characteristics of the pure spinel electrode. With increasing spinel content a decrease in potential drop is seen. For a base current rate of 0.1C, the data curves of spinel and both blends show comparable characteristics with no significant change in potential drop, up to 80% DoD, while at 3C this point shifts to 40% DoD. The extent of divergence in potential drop is strongly dependent on the base C-rate and the blend ratio. The characteristics of both blends cannot be fully explained assuming pure physical mixtures. The observed potential drop is below the expected values and can be partially ascribed to a lower electrode polarization due to faster kinetics at the manganese plateau. In addition, a possible interaction between LFMP and spinel particles is likely because the blend electrodes entirely resemble the characteristics of the spinel electrode. The results also show that blending LFMP with spinel by 50 cap% results in a cathode that is able to accommodate high power pulses. For the

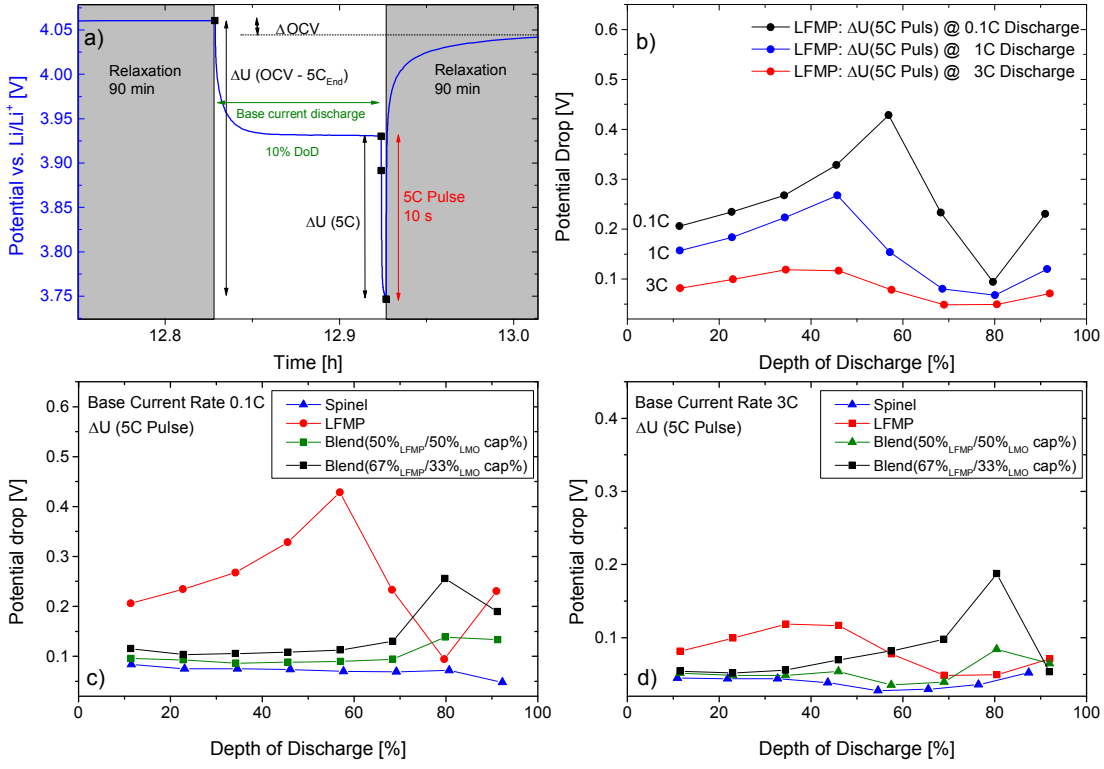

Fig. 6. a) Schematic of power pulse test evaluation b) Potential drops of LFMP caused by 5C pulses according to the applied base current rate. Potential drop of LFMP, spinel and both blends caused by 5C pulses according to the applied base current rate for rates of a) 0.1C and d) 3C.

investigated electrodes, a higher pulse capability can be observed up to 70% DoD.

3.7. Manganese dissolution

Manganese dissolution of the spinel structure is one of the major problems in spinel-based Lithium-Ion-Batteries. It affects the stability of the cell and can deteriorate the anode [18]. Therefore, manganese dissolution plays an important roll for cell lifetime. The used spinel contains ca. 1.5 wt% of aluminum in order to increase the stability of the material against structural changes and manganese dissolution [15]. A reduced manganese release is also reported for blends of spinel and $LiNi_{0.8}Co_{0.15}Al_{0.05}O_2$ (NCA) [19,20]. To address this practical demand, we investigate the influence of the spinel to olivine ratio on the amount of dissolved manganese. Electrodes of different blend ratios as well as the pure spinel and pure LFMP are stored in electrolyte (EC:DMC = 1:1, 1 M $LiPF_6$) for two weeks at 60 °C. The amount of dissolved manganese in the electrolyte is determined by ICP-OES measurements and the results are depicted in Fig. 7. Low manganese dissolution is shown for the pure olivine (0 wt% spinel), with a value of 0.32 mg per kg electrolyte. For pure spinel, a total amount of 75 mg manganese per kilogram electrolyte can be detected, which is more than two magnitudes higher as compared to LFMP. Fig. 7 depicts measured and theoretical values. The latter have been calculated assuming pure physical mixtures. For all blends, the experimental data show a drastically reduced manganese dissolution compared to theoretical values. According to their amount of spinel, the measured values can be fitted with an exponential curve. The reduced solubility of manganese might be due to the basic character of the LFMP surface. Experimental data reveal an increase in pH of 1.5 when soaking 500 mg LFMP in 2 g of demineralized water in contrast to pure water. Therefore two possible explanations can be discussed both of which are related to scavenging effects: 1) either the catalytic circle described by Hunter [21] is interrupted when protons are neutralized by the basic surface of LFMP or 2) dissolved manganese can be re-precipitated on the alkaline surface of the LFMP particles.

Fig. 8 compares the battery relevant features of LFMP, spinel and the blend. In general for a blend material, each component is expected to contribute according to their ratio within the electrode, as in the case for pure physical mixtures. In our case the capacity contribution of LFMP and spinel in this blend is $50_{LFMP}/50_{LMO}$ cap%. We expect an equal contribution of both materials. In terms of tap density, this behavior can be observed. For all other features the mean value can be surmounted demonstrating the power of positive synergetic effects in this kind of blend electrodes.

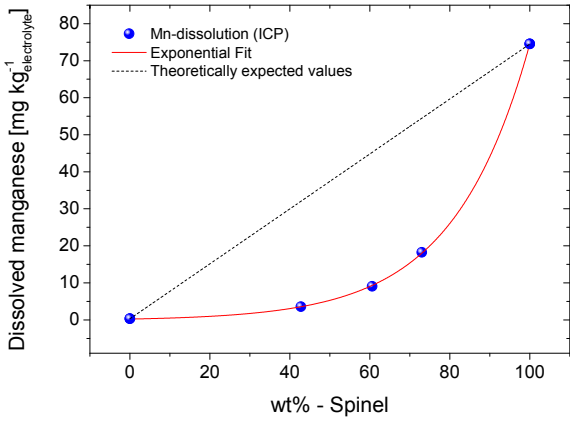

Fig. 7. Amount of manganese dissolved in one kg Electrolyte after a storage time of 2 weeks at 60 °C relating to the spinel ratio.

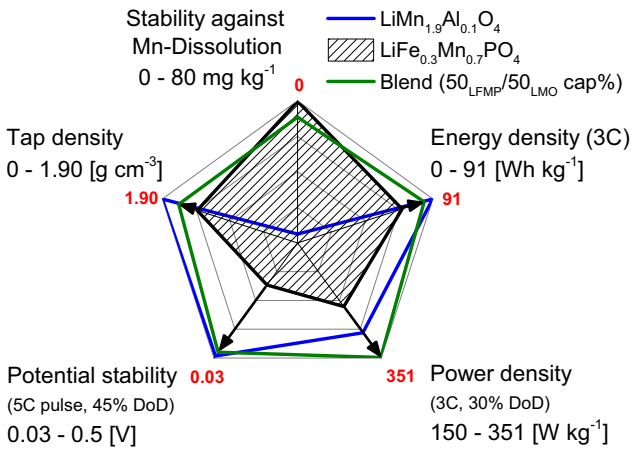

Fig. 8. Radar chart comparing relevant material features of LMFP, spinel and Blend($50_{LFMP}/50_{LMO}$ cap%).

4. Conclusion

LFMP is an electrochemically stable cathode material delivering high energy densities but suffering from low kinetics on the manganese redox step. Blending LFMP with spinel is a promising way to overcome these issues. Different blend ratios are prepared and characterized according to their physical and electrochemical behavior. All results are discussed relating to pure LFMP as well as pure spinel and differences are elaborated. Blend properties as tap density, capacity, energy density and power density at low C-rates follow physical mixtures in their behavior. Synergetic effects can be assumed for potentials at high rates and power densities at high states of charge. Enhanced pulse power capability can be detected as result of reduced electrode polarization. Furthermore, a drastic reduction in manganese dissolution can be observed for blend electrodes due to the alkaline character of LFMP. These complementary properties of the single component materials LFMP and spinel result in a cathode material which is promising for starter batteries in automotive applications, where high power densities at high states of charge are required in order to start the internal combustion engine.

Acknowledgment

The authors wish to thank Gisela Arnold for analytical support and Stephanie Fleischmann for fruitful discussions. We also want to thank Johnson Matthey Battery Materials GmbH for providing the LFMP. The present work was partially supported by BMBF BASTA (03X4628A) and LiEcoSafe (03X4636A).

Appendix A. Supplementary data

Supplementary data related to this article can be found at http://dx.doi.org/10.1016/j.jpowsour.2016.01.093.

References

[1] A.K. Padhi, K.S. Nanjundaswamy, J.B. Goodenough, Phospho-olivines as positive-electrode materials for rechargeable lithium batteries, J. Electrochem. Soc. 144 (4) (1997) 1188–1194.
[2] G. Li, H. Azuma, M. Tohda, $LiMnPO_4$ as the cathode for lithium batteries, Electrochem. Solid State Lett. 5 (2002) A135–A137.

[3] A. Yamada, Y. Kudo, K.-Y. Liu, Reaction mechanism of the olivine-type $Li_x(Mn_{0.6}Fe_{0.4})PO_4$ ($0 \leq x \leq 1$), J. Electrochem. Soc. 148 (7) (2001) A747–A754.
[4] A. Yamada, K. Yoshihiro, K.-Y. Liu, Phase diagram of $Li_x(Mn_yFe_{1-y})PO_4$ ($0 \leq x, y \leq 1$), J. Electrochem. Soc. 148 (10) (2001) A1153–A1158.
[5] K.G. Gallagher, S.-H. Kang, S.U. Park, S.Y. Han, $xLi_2MnO_3 \cdot (1-x)LiMO_2$ blended with $LiFePO_4$ to achieve high energy density and pulse power capability, J. Power Sources 196 (2011) 9702–9707.
[6] J.F. Whitacre, K. Zaghib, W.C. West, B.V. Ratnakumar, Dual active material composite cathode structures for Li-ion batteries, J. Power Sources 177 (2008) 528–536.
[7] S.B. Chikkannanavar, D.M. Bernardi, L. Liu, A review of blended cathode materials for use in Li-ion batteries, J. Power Sources 248 (2014) 91–100.
[8] R.J. Gummow, A. de Kock, M.M. Thackeray, Improved capacity retention in rechargeable 4 V lithium/lithium-manganese oxide (spinel) cells, Solid State Ionics 69 (1) (1994) 59–67.
[9] T. Ohzuku, M. Kitagawa, T. Hirai, Electrochemistry of manganese dioxide in lithium nonaqueous cell. III. X-ray diffractional study on the reduction of spinel-related manganese dioxide, J. Electrochem. Soc. 137 (3) (1990) 769–775.
[10] M. Hosoya, H. Ikuta, T. Uchida, M. Wakihara, The defect structure model in nonstoichiometric $LiMn_2O_{4-\delta}$, J. Electrochem. Soc. 144 (4) (1997) L52–L53.
[11] D.H. Jang, Y.J. Shin, S.M. Oh, Dissolution of spinel oxides and capacity losses in 4 V $Li/Li_xMn_2O_4$ cells, J. Electrochem. Soc. 143 (1996) 2204.
[12] D.H. Jang, S.M. Oh, Electrolyte effects on spinel dissolution and cathodic capacity losses in 4 V $Li/Li_xMn_2O_4$ rechargeable cells, J. Electrochem. Soc. 144 (10) (1997) 3342–3348.
[13] Y. Xia, M. Yoshio, An investigation of lithium ion insertion into spinel structure Li-Mn-O compounds, J. Electrochem. Soc. 143 (3) (1996) 825–833.
[14] M.M. Thackeray, Manganese oxides for lithium batteries, Prog. Solid State Chem. 25 (1997) 1–71.
[15] D. Song, H. Ikuta, T. Uchida, M. Wakihara, The spinel phases $LiAl_yMn_{2-y}O_4$ (y=0, 1/12, 1/9, 1/6, 1/3) and $Li(Al,M)_{1/6}Mn_{11/6}O_4$ (M=Cr, Co) as the cathode for rechargeable lithium batteries, Solid State Ionics 117 (1) (1999) 151–156.
[16] S.-T. Myung, S. Komaba, N. Kumagai, Enhanced structural stability and cyclability of Al-doped $LiMn_2O_4$ spinel synthesized by the emulsion drying method, J. Electrochem. Soc. 148 (5) (2001) A482–A489.
[17] J.-P. Schmidt, H.Y. Tran, J. Richter, E. Ivers-Tiffée, M. Wohlfahrt-Mehrens, Analysis and prediction of the open circuit potential of lithium-ion cells, J. Power Sources 239 (2013) 696–704.
[18] T. Aoshima, K. Okahara, C. Kiyohara, K. Shizuka, Mechanisms of manganese spinels dissolution and capacity fade at high temperature, J. Power Sources 97–98 (2001) 377–380.
[19] H.Y. Tran, C. Täubert, M. Fleischhammer, P. Axmann, L. Küppers, M. Wohlfahrt-Mehrens, $LiMn_2O_4$ spinel/$LiNi_{0.8}Co_{0.15}Al_{0.05}O_2$ blends as cathode materials for lithium-ion batteries, J. Electrochem. Soc. 158 (5) (2011) A556–A561.
[20] T. Numata, C. Amemiya, T. Kumeuchi, M. Shirakata, M. Yonezawa, Advantages of blending $LiNi_{0.8}Co_{0.2}O_2$ into $Li_{1+x}Mn_{2-x}O_4$ cathodes, J. Power Sources 97–98 (2001) 358–360.
[21] J.C. Hunter, Preparation of a new crystal form of manganese dioxide: λ-MnO_2, J. Solid State Chem. 39 (2) (1981) 142–147.